SCIENCE CHINA
Technological Sciences

December 2013 Vol.56 No.12: 2934–2952
doi: 10.1007/s11431-013-5404-1

Study on microscale adhesion between solid surfaces with scanning probe

LAI TianMao & HUANG Ping*

School of Mechanical and Automotive Engineering, South China University of Technology, Guangzhou 510640, China

Received September 1, 2013; accepted October 20, 2013; published online October 31, 2013

The adhesion between two parallel solid surfaces is of great interest with the rapid development of micro-nano devices and instruments. The adhesion forces between a flat tip with a diameter ~1.7 μm and some surface have been determined by recording the force-displacement curves with an atomic force microscope (AFM). The flat tip is used to prevent wear and mimic the adhesion between two parallel surfaces. The free energy of the solid surface is calculated by the contact angles between the probe liquids and the surface. The adhesion force between parallel solid surfaces cannot be predicted by the theory of thermodynamic surface free energy. The adhesion measurements were carried out under ambient conditions, in a nitrogen-filled glove box, under distilled water, and under potassium chloride (KCl) solution. The outcome shows that the real contact area without the applied load is only a small proportion of the apparent contact area. The measurement stability and repeatability of adhesion by the AFM depend on the surface characterization, measurement methods and the environment. Under different environments, there are different interactions and factors affecting the adhesion force, and the dominant interactions and factors may be different too. The various interactions and factors are mutually coupled to determine the final adhesion force.

micro-scale, adhesion force, atomic force microscope, force-displacement curve, flat tip, surface free energy

Citation: LaI T M, Huang P. Study on microscale adhesion between solid surfaces with scanning probe. Sci China Tech Sci, 2013, 56: 2934–2952, doi: 10.1007/s11431-013-5404-1

1 Introduction

The adhesion property between two parallel solid surfaces is of great interest in many scientific and industrial fields. With the rapid development of micro-scale/nano-scale devices and instruments, this kind of adhesion becomes more and more important. The small-scale mechanical systems have high surface-area-to-volume ratios. Therefore, these systems are more influenced by surface effects rather than inertia effects. The adhesion force is the chief factor of the failures of micro electro mechanical systems (MEMS) in the manufacture and in use [1]. Meanwhile, in order to further the practicability and miniaturization of MEMS, it is urgent to develop a sophisticated understanding and control of adhesion between solid-solid surfaces.

There are two major methods to describe and predict the adhesion force. One is to determine the thermodynamic work of adhesion, while the other is to determine the magnitude of the fundamental forces and sum these forces. In the first method, the work of adhesion is defined as the work required separating two surfaces from contact to infinite separation. The work of adhesion is related to the surface free energies of the surfaces and the media between them [2]. And, many methods can be used to calculate the free energy of the solid surface by the contact angles between probe liquids and the surface. After the contact of two surfaces, they are inevitably deformed due to their finite elasticity. There are some contact mechanics models that can be used to determine the adhesion force by using the

*Corresponding author (email: mephuang@scut.edu.cn)

work of adhesion. These models include Johnson-Kendall-Roberts (JKR) model [3], Derjaguin-Muller-Toporov (DMT) model [4], Maugis-Dugdale (MD) model [5], etc. However, these theories only relate the work of adhesion and the adhesion between a sphere and a flat surface. The appropriate theory used depends on the material properties, the size of the sphere, and the normal applied load.

In the second method, the fundamental forces are added to determine the final adhesion force. At the molecular scale, the adhesion is extremely complex and may involve different physical and chemical mechanisms. Different contributing mechanisms are usually formed as a whole to determine the final adhesion force. In the most general case, the adhesion force is a combination of the electrostatic force, the van der Waals (vdW) force, the capillary force and forces due to chemical bonds or acid-base interactions [6]. In some special cases, a single mechanism may also become the dominant factor.

Under different conditions, the dominant factors of adhesion may be different. Under ambient conditions, the capillary force is always present due to capillary condensation and adsorption of thin water films on surfaces. This interaction depends on the relative humidity and the hydrophilicity of the surfaces. In dry gaseous environments, the capillary force will disappear, and the vdW force and electrostatic forces may become the dominant forces. In particular, the electrostatic forces can be large on insulators, since the charge dissipation is ineffective at low humidity. Under distilled water, there is in general no capillary force or electrostatic forces. And the significant contribution is from the vdW force. However, in aqueous solutions, most surfaces become charged due to dissociation of surfaces groups, and the electrostatic double layer interactions are important. The magnitude of double-layer force depends on electrolyte concentration. If the chemical end-groups are present on the surfaces, chemical bonds may form during contact or other chemical interactions may occur. In the presence of chemical bonds, forces due to chemical bonds are generally believed to dominate the adhesion force. Of course, the vdW forces are always present in all systems. There may be some other forces in the system, such as hydrophobic forces, structural forces, depletion forces and so on. However, these forces apply to very specific systems. For example, the hydrophobic force will only be present between two highly hydrophobic surfaces, and structural forces are the strongest between highly idealized surfaces [7].

Not only exist many adhesion mechanisms, but also various parameters can influence adhesion. These parameters include surface roughness, hydrophilicity, temperature, humidity, etc. Roughness has a significant effect on adhesion. Surface roughness decreases the actual contact area. As a consequence, the adhesion is reduced. The efficiency of the decrease in real contact area for the reduction of adhesion has been investigated in detail by a lot of researchers. And attempts to find a critical surface roughness to obtain the minimum of adhesion have also been reported [8, 9]. Generally, the impact of relative humidity on adhesion is reflected through the capillary force and vdW force [10]. When the relative humidity is below 10%, the adhesion remains unchanged, and is mainly contributed by the vdW interaction. With increasing humidity, the adhesion force then increases and remains constant due to capillary forces and the vdW forces. The adhesion force then decreases at very high relative humidity.

In order to reduce and control the adhesion force, measuring the adhesion force is required in advance. There are many apparatuses to measure adhesion at the microscopic scale, such as surface force apparatus (SFA), interfacial force microscope (IFM), atomic force microscopy (AFM), and so on. Among them, the AFM has been widely used for adhesion force measuremen. It provides a simple and accurate way to determine adhesion force with high spatial resolution. It is possible to measure adhesion force between any types of surfaces in any environment. The adhesion force can also be correlated with topography measurements. And the AFM is less subject to contamination than other methods. The adhesion force between the tip and sample is determined by recording a force-displacement curve. The force-displacement curve is obtained by monitoring the deflection of a cantilever as the tip approaches and retracts from the sample. First measurements of adhesion forces by the AFM were performed by Martin et al. [11] and Erlandson et al. [12]. So far, the measurement technology of the AFM has been fully developed and widely used to measure a variety of surface forces in surface science, materials engineering, biotechnology, medicine, and so on [13–18].

To measure the adhesion force by the AFM, the tip shape is always known beforehand. In general, the traditional probe tip has a parabolic shape with an end radius varying from 10 to 100 nm. In many situations, the asperities have geometries that may be better described by a power-law function, instead of having paraboloidal shapes [19]. A serious disadvantage of sharp tips in measuring adhesion is the wear of the tips [20]. Sharp tips wear easily, resulting in the variation of the contact area between the tip and sample. If the real area of contact is not well defined, then quantification of the adhesion force will become difficult. The shortcoming can be overcomed by the introduction of colloid probe technique [21]. A spherical particle can be attached to the end of a cantilever. The accessible range of particle size is typically limited to a range between 1 and 50 μm. This kind of probe has become a well-established tool for studying adhesion due to its defined geometric shape and wear resistance.

A probe tip with a large and flat cylindrical end can not only overcome the shortcoming, but also be used to mimic a flat surface. However, this kind of tip has only been used in a few experiments to study the adhesion forces. By using a tip having a flat, square surface measuring 0.7 μm × 0.7 μm, Ando [22] measured the adhesion forces between the tip

and the hemispherical asperity arrays on Si produced by focused ion beam. In a subsequent publication, Ando [23] studied the adhesion forces between a Ni tip with a 0.1 μm^2 flat area and a flat Si substrate. Ferreira et al. [24] used a flat probe tip to measure the adhesion force. The results showed that the combination of materials characteristics, testing geometry and experimental protocol (contact time, contact force and contact area) have a great influence on the adhesion force. Colak et al. [25] used a flat tip with a diameter of 2 μm to measure the adhesion forces between the tip and a smooth and chemically etched Si (1 0 0) surface.

In this paper, the adhesion forces between two parallel solid surfaces will be determined by recording force-displacement curves with the AFM. A flat tip will be used to measure the adhesion forces of six different samples under four different environments. The free energy of the sample surfaces are calculated by the contact angles between the probe liquids and the surfaces. We will also study the influence of numerous measurements, the normal applied load and the contact time on the adhesion force at a single location. In order to obtain mean adhesion forces and the distribution, a number of locations will be selected to record adhesion forces in a scanning area. The mean adhesion forces and the distributions will be investigated to analyze the affecting factors under different conditions. The results of this paper can provide a reference to the design and manufacture of micro-nano devices and instruments.

2 Experimental methods

2.1 Samples preparation

There are 6 samples used in the experiments. Sample 1 (polished Si) is an N-type polished silicon wafer of (100) orientation. The thickness of it is 400±10 μm, and the resistivity is 5–10 Ω cm. The sample is cleaned by the hydrofluoric acid (HF) to remove the natural oxide layer on the sample. Sample 2 (oxidized Si) is covered with a silicon dioxide film by thermal growth method from the polished Si. The thickness of the oxide layer is 500±20 nm. Sample 3(etched Si) is obtained from the polished Si by the anisotropic etching method. The etchant used is the mixture of the potassium hydroxide (KOH, 25% mass fraction) and isopropanol. The silicon is oxidized to yield a silicon compound, and the silicon compound reacts with the isopropanol to form a soluble silicon complex. The reaction mechanism is as follows:

$$\mathrm{KOH + H_2O \rightarrow K^+ + 2OH^- + H^+} \quad (1)$$

$$\mathrm{Si + 2OH^- + 4H_2O \rightarrow Si(OH)_6^{2-} + 2H_2}\uparrow \quad (2)$$

$$\mathrm{Si(OH)_6^{2-} + 6(CH_3)_2CHOH \rightarrow [Si(OC_3H_7)_6]^{2-} + 6H_2O} \quad (3)$$

Sample 4 (grooved Si) is grinded from the polished Si by a grinding wheel with diamond particles [26]. Samples 5 and 6 are sapphire (Al_2O_3) and quartz (SiO_2), respectively. Before the experiments, all the samples were ultrasonically cleaned in an alcohol solution for 15 minutes, and then ultrasonically cleaned in the distilled water for 15 minutes.

2.2 Atomic force microscope and measurement method

The experiments were performed by using an atomic force microscope of beam deflection type (AFM, Being Nano-Instruments CSPM-4000, China). The microscope was operated under distilled water (temperature 28±1°C), under 1 mol/L potassium chloride (KCl) solution (temperature 28±1°C), under ambient conditions (temperature 28± 1°C, relative humidity 65±2%) and in a glove box (Etelux Lab2000) where the water content and oxygen content were all less than 0.1 ppm (temperature 31±1°C).

The schematic diagram of the AFM is shown in Figure 1. It consists of the laser source, the quadrant photo-detector, the probe, the piezo scanner, the controller and the computer. The scanner consists of piezoelectric ceramic tubes with three directions. In the scanning process, the scanner (carrying the sample) moves up and down, left and right, front and rear by the control voltages, while the probe is fixed to a probe base. The laser emitted by the laser source is reflected by the back of the cantilever, and the reflected light is received by the quadrant photo-detector. The difference in signal between the top and bottom quadrants of photodector, $(A+B)-(C+D)$, represents the vertical deflection of the cantilever. Meanwhile, the left and right quadrants of photodector, $(A+C)-(B+D)$, are used to measure the torsional deformation of the cantilever.

The AFM liquid phase mode can be used to measure the adhesion force under the liquid. A diagram of the structure is shown in Figure 2. A piece of quartz glass is added above the probe, and the liquid is between the glass and the sample. The probe is completely submerged under the liquid. The laser can reach the back of the cantilever after the refraction

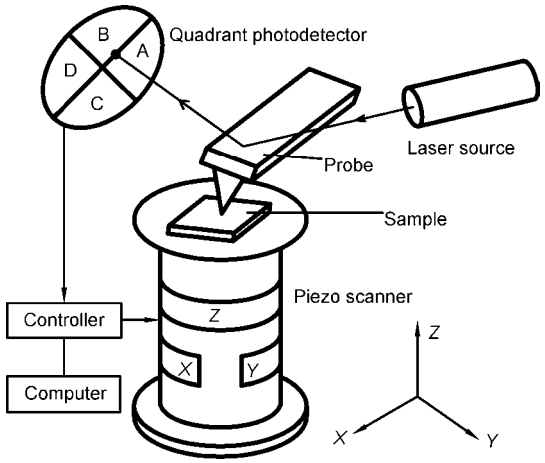

Figure 1 Diagram of the atomic force microscope.

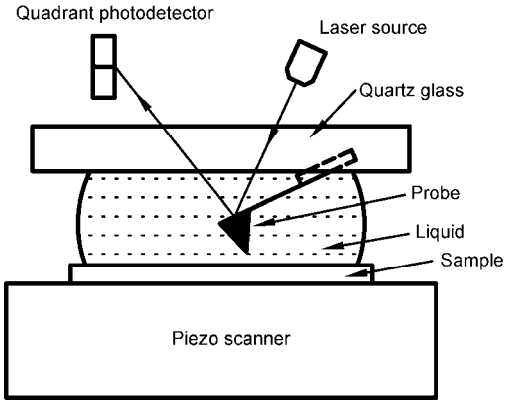

Figure 2 Schematic representation of the liquid phase mode of the AFM.

of the glass and the liquid.

Two different probes are used in these experiments. The first probe is a rotated monolithic silicon probe (ContAl, Budget Sensors). Its tip radius is less than 10 nm, and it is used to measure the surface roughness of the samples. The second probe is a single crystalline silicon probe (PL2-CONTR by Nanosensors, Switzerland). As is shown in Figure 3, an intentionally blunt tip with a well-defined circular end-face is located at the free end of a rectangular cantilever. The flat tip is formed by focused ion beam milling and has a 1.73 μm diameter contact area. The tip shapes and other geometric values of cantilevers were determined by using a scanning electron microscopy (SEM) (Hitachi S-3700N, Tokyo, Japan). The force calibration is accomplished by its geometrical parameters. The width, thickness, length of the cantilever and the tip height are w=44 μm, t=1.9 μm, l=456 μm and h=18.5 μm, respectively. The elastic modulus of the tip is $E = 1.69\times10^{11}$ N/m^2. The normal spring constant can be calculated based on these parameters [27]:

$$C_{\mathrm{N}} = \frac{Ewt^3}{4l^3} = 0.135 \text{ N/m}. \quad (4)$$

In the AFM, the adhesion force is obtained by the force-displacement curve. During the measurement, the probe is fixed, and the scanner moves up and down by Z-direction driving voltages. So the tip and the sample are in contact and then are separated with each other, successively. The force-displacement curve is obtained by recording the Z-direction voltage of the scanner and the voltage of quadrant photodetector. A typical force-displacement curve is shown in Figure 4.

The horizontal axis represents the Z-direction voltage of the scanner U_{SZ} or scanner displacement D_{SZ}. An proportional relationship between them exists: $D_{\mathrm{SZ}} = E_{\mathrm{Z}}U_{\mathrm{SZ}}$, where E_{Z} (nm/V) is the extension coefficient of the scanner in the Z direction. The vertical axis represents the voltage of quadrant photodetector or cantilever deflection or tip-sample interaction force. Proportional relationships among them exist, too. The figure also schematically shows the scanner positions and the light spots on quadrant photodetector corresponding to the points on the curve.

As shown in Figure 4, the approaching process is from point A to point E. (A) The tip is still far away from the sample. The voltage of quadrant photodetector is zero, and the cantilever is in a free state (no measurable interaction is detected between the tip and sample). The zero line is defined as a part of the force-displacement curve, in which the tip exerts no force on the sample. Upon approaching the surface, the tip may sense attractive forces or repulsive forces, which cause the end of the cantilever to bend downward or upward (not shown in the figure). (B) If the force gradient of the short-range attractive tip-sample interaction force exceeds the normal spring constant of the cantilever, the tip will snap into contact (C) with the sample. The tip and sample will keep in contact after that. As the sample moves up continuously, the curve eventually crosses

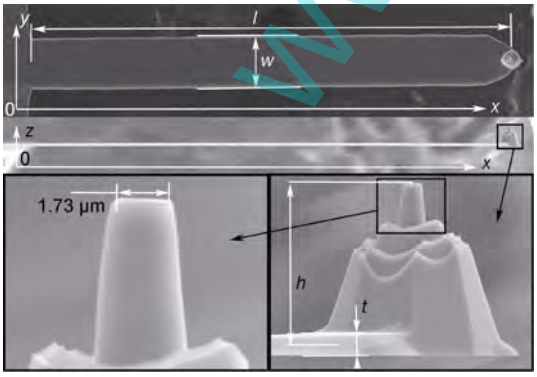

Figure 3 Scanning electron microscope image of the probe with a plateau tip. The coordinates and geometrical parameters are shown.

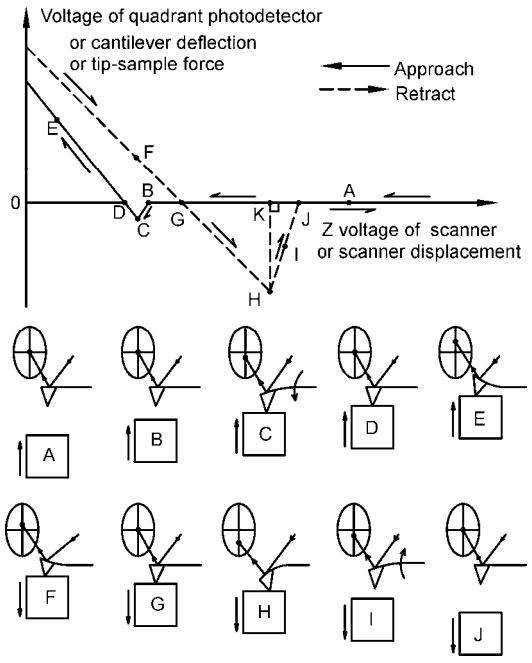

Figure 4 A typical force-displacement curve and the relative positions of tip and scanner.

the zero line (D). At this point, the voltage of quadrant photodetector is zero again. As the sample continues to move up, the cantilever bends upward, and the lever-sample interaction continues to increase (E is one of the points), until a predetermined voltage of the scanner is reached. If the surface of the sample is soft, a sharp probe tip may be engraved into the surface.

After reaching the maximum voltage of the scanner, the voltage will began to decrease, and the scanner moves down. The retraction of the sample will lead to the reverse process (F-J). In this process, the tip-sample interaction continues to decrease. At point G, the voltage of quadrant photodetector is zero again. Then, the interaction becomes negative without withdrawal of the tip, since the adhesion force between the tip and sample maintains the contact. When the normal spring constant of the cantilever exceeds the force gradient of the interaction, the tip immediately snaps out of contact with the sample (H). This instability is always thought of as a fracture process. Subsequently, the cantilever goes back to its original starting position (I-J).

The adhesion force can be obtained by the force-displacement curve. In Figure 4, if the vertical axis represents tip-sample interaction force, then the segment HK represents the adhesion force. However, the signals recorded by the AFM are the Z-direction voltage of the scanner U_{SZ} and the voltage of quadrant photodetector U_N. Therefore, U_N should be converted into the cantilever deflection, and finally into force. This conversion is accomplished by the sensitivity. The sensitivity S_Z (dimensionless) is the ratio of the difference of the scanner Z-direction voltage to the difference voltage of quadrant photodetector, i.e., $S_Z = U_{SZ}/U_N$. If the tip is not carved into the surface and the elastic deformation of the sample is negligible (measurement on hard surfaces, such as Al_2O_3), the vertical movement of the scanner equals the deflection of the cantilever, that is, $\delta_N = D_{SZ} = E_Z U_{SZ}$. Then we have $\delta_N = E_Z U_{SZ} = E_Z S_Z U_N$. If the horizontal and vertical coordinates represent the voltage signals, a straight line parallel to the two slashes can be drawn. The cotangent of the closed angle between the line and the horizontal is the required sensitivity. The adhesive force can be expressed as

$$F_{ad} = C_N \delta_N = C_N E_Z S_Z U_N, \tag{5}$$

where U_N is the voltage difference represented by the segment HK.

When the Z-direction voltage of the scanner reaches the maximum, it will begin to decrease. That is, there is a maximum loading force between the tip and sample F_N. This force can be calculated as

$$F_N = C_N E_Z U_{0D}, \tag{6}$$

where U_{0D} is the voltage difference represented by the segment 0D on the horizontal axis.

It is worthwhile to note that the pull-off force is not the adhesive bond strength [28]. In other words, it is not a direct measure of the actual adhesive forces that were acting between the tip and sample in the absence of loading force. However, if the normal spring constant is sufficiently low and the long-range attractive force is small, the adhesion force measured by the AFM does nearly correspond to the maximum attractive force. That is why we choose a soft cantilever (C_N= 0.135 N/m).

2.3 Contact angle measurements

The contact angles were measured by JC2000A contact angle goniometer (Powereach, Shanghai, China). Four probe liquids with different surface tensions and surface tension components (diiodomethane, ethyleneglycol, glycerol, and distilled water) were used for these measurements. The contact angles were measured for at least 5 liquid drops having a base diameter from 4 to 6 mm. All measurements were conducted at room temperature, 26–28°C.

3 Results and discussion

3.1 Sample surface characterization: Topographical analysis

The surface topographies of the samples have been determined from imaged areas of 60 μm×60 μm which are the representative of the samples, as shown in Figure 5. The first probe with tip radius less than 10 nm was used to measure the surface topographies by contact mode. The histograms of surface height distributions are shown in Figure 6. Each of them exhibits a Gaussian-like distribution.

The surface roughness is quantified using two parameters of roughness: average roughness R_a and root-mean-square roughness R_q [29]. The parameters are defined by

$$R_a = \frac{1}{n}\sum_{i=1}^{n}\left|z_i - z_{ave}\right|, \tag{7}$$

$$R_q = \sqrt{\frac{1}{n}\left[\sum_{i=1}^{n}\left(z_i - z_{ave}\right)^2\right]}, \tag{8}$$

where z_i is the topographic height at point i, n is the number of points measured within the area, z_{ave} is the average value of topographic heights within the area, $z_{ave} = \left(\sum_{i=1}^{n} z_i\right)/n$. Table 1 shows the results of the roughness analysis of the samples.

3.2 Sample surface characterization: Surface free energy

There are many methods to calculate the surface free energy of the solid by contact angles. The method proposed by

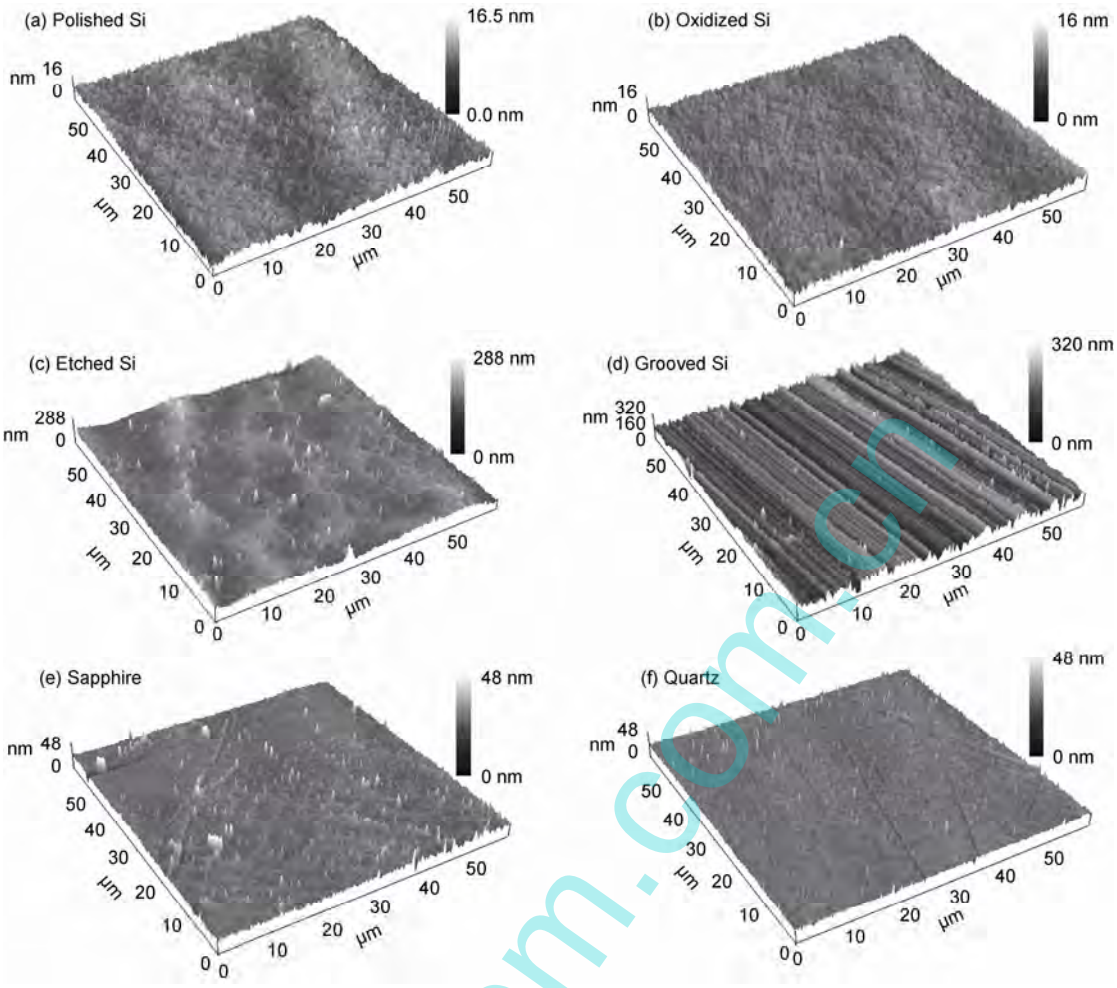

Figure 5 Topographic AFM images of all the samples. Scanning areas are all 60 μm×60 μm.

Owens and Wendt [30] is used in the calculations here. The relationship between the contact angle and the surface tension is $\cos\theta = (\gamma_S - \gamma_{SL})/\gamma_L$, where θ is the contact angle, γ_S and γ_L are the surface tensions of solid and liquid surfaces, respectively, γ_{SL} is the solid-liquid interfacial tension. Fowkes [31] proposed that the surface tension can be decomposed into two components, $\gamma = \gamma^d + \gamma^p$, where γ^d and γ^p are the dispersive component and polar component. Furthermore, Owens and Wendt [30] introduced a semi-empirical formula:

$$\gamma_L(1+\cos\theta) = 2(\sqrt{\gamma_S^d \gamma_L^d} + \sqrt{\gamma_S^p \gamma_L^p}), \quad (9)$$

where superscripts d and p represent the dispersion and polar components, respectively, while subscripts S and L represent the solid and liquid, respectively. It can be seen from the above equation that in order to calculate the solid surface free energy, the components of the surface free energies of the probe liquids must be known. The components of the four liquids reported in the literature are used here, as shown in Table 2.

Eq. (9) can be further simplified into

$$y = x\sqrt{\gamma_S^p} + \sqrt{\gamma_S^d}, \quad (10)$$

where $x = \sqrt{\gamma_L^p}/\sqrt{\gamma_L^d}$ and $y = \gamma_L(1+\cos\theta)/(2\sqrt{\gamma_L^d})$. The values of x and y can be calculated from the contact angle and the surface free energy components for each probe liquid. A straight line representing eq. (10) can be drawn by the linear fit based on the scatter points of x and y. The slope of the line is $\sqrt{\gamma_S^p}$, while the y-axis intercept is $\sqrt{\gamma_S^d}$. The calculation of the surface free energy of polished Si with this method is shown in Figure 7. The free energies of the other samples are calculated by the same method. Table 3 shows the contact angles and surface free energies of the samples. As can be seen from it, there is a little difference among the surface energies of the samples. It seems that the change of the surface energy of the silicon wafer is small after etching or grooving.

3.3 Influence of the number of contacts on adhesion force

When recording force-displacement curves to obtain adhe-

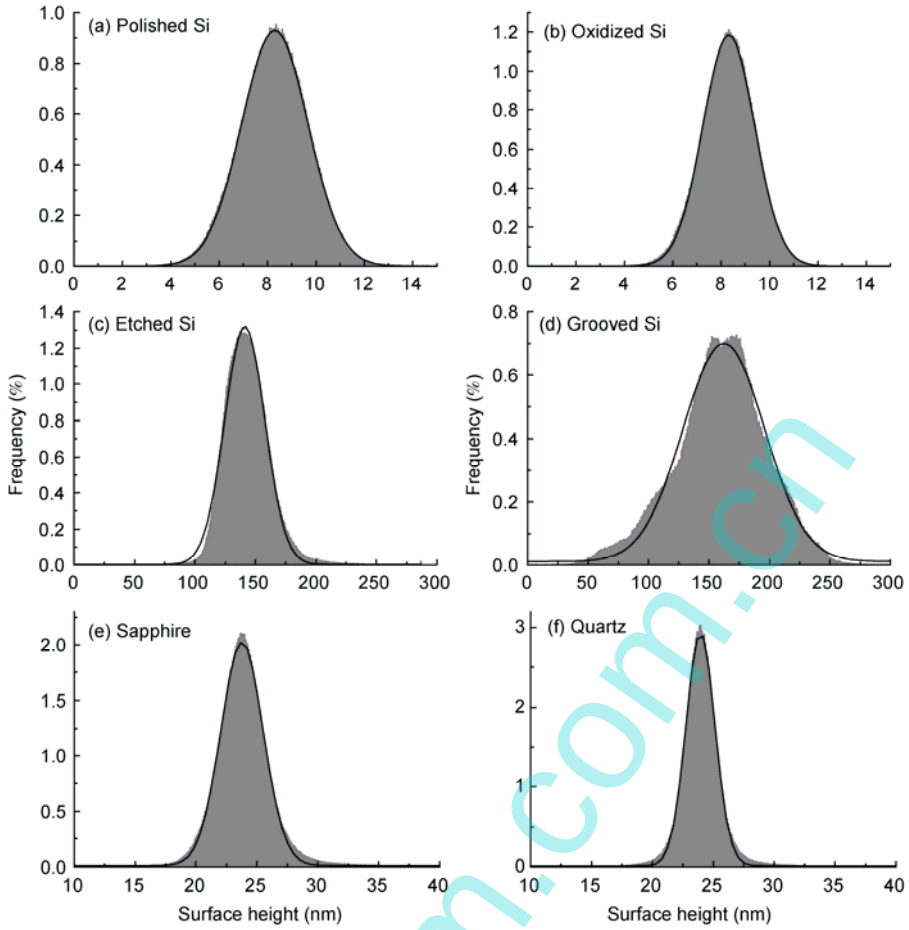

Figure 6 Histograms of surface height distributions.

Table 1 Roughness analysis of the samples (see eqs. (7), (8) for definitions of the parameters)

Sample number	Sample name	R_a (nm) (3.6×10^3 μm^2)	R_q (nm) (3.6×10^3 μm^2)
1	Polished Si	1.11	1.41
2	Oxidized Si	0.87	1.1
3	Etched Si	16.7	21.9
4	Grooved Si	29.5	37.6
5	Sapphire	1.73	2.61
6	Quartz	1.23	1.96

Table 2 Surface free energies and components of various probe liquids

Probe liquid	γ_L (mJ m^{-2})	γ^d_L (mJ m^{-2})	γ^p_L (mJ m^{-2})	Reference
Diiodomethane	50.8	48.5	2.3	[32]
Ethyleneglycol	47.7	30.1	17.6	[32]
Glycerol	64.0	34.0	30.0	[33]
Water	72.8	21.8	51.0	[33]

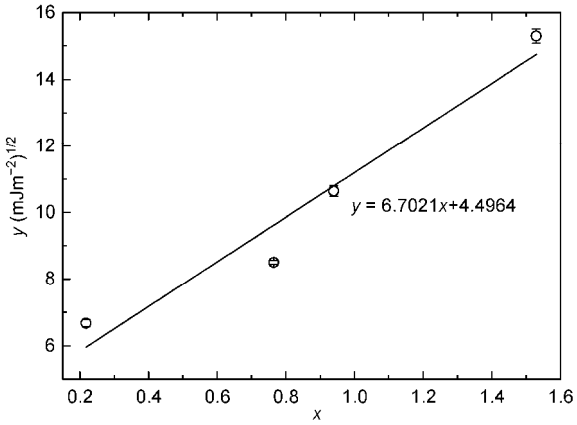

Figure 7 The calculation of the surface free energy of polished Si with linear fitting method. Each point is an average of at least five measurements, the error bar being the standard deviation of each set of points.

sion forces, an important question is whether the adhesion from the first contact is different from the ones from subsequent contacts. Therefore, the adhesion forces were measured 128 or 256 times at a single location to examine the reproducibility of the adhesion measurements. The variation of adhesion was examined with the sequential measurements. The experiments were carried out in a glove box, under ambient conditions (after being taken out of the glove box and exposure for two hours) and under distilled water. The applied load was ~220 nN, and the contact time was 0 s.

Table 3 Contact angles and surface free energies of the samples

Sample	Diiodomethane (°)	Ethyleneglycol (°)	Glycerol (°)	Water (°)	γ^d_s (mJ m^{-2})	γ^p_s (mJ m^{-2})	γ_s (mJ m^{-2})
Polished Si	33.8±3.0	16.7±2.8	19.7±4.3	14.9±5.7	20.2	44.9	65.1
Oxidized Si	37.5±2.9	16.1±5.8	30.7±5.5	16.3±3.4	18.6	45.6	64.2
Etched Si	36.0±3.1	12.6±2.2	21.7±1.9	15.0±4.5	19.6	45.8	65.4
Grooved Si	35.9±1.9	12.3±3.9	28.2±12.4	21.9±2.4	20.4	42.4	62.8
Sapphire	37.4±2.8	12.8±2.2	28.5±6.5	16.6±3.6	19.0	45.4	64.4
Quartz	35.4±2.6	20.6±3.7	25.4±5.8	18.2±3.7	19.5	44.4	63.9

Figure 8 shows the adhesion forces depending on the number of contacts in the glove box. With the increase of the measurement number, the adhesion forces of polished Si and oxidized Si increase slightly. The fluctuation of adhesion forces is small, since the average and standard deviation of adhesion are 86.78±4.01 nN and 56.61±2.52 nN, respectively. The adhesion forces of sapphire (92.65±7.84 nN) are divided into two parts (near 80 and 100 nN, respectively), which are also with small fluctuations. However, the adhesion forces of quartz (110.32±15.02 nN) steppedly increase with the increasing of the measurement number. This is most likely due to the plastic deformation or damage of the asperities on the surface.

Figure 9 shows the adhesion variations of etched Si and grooved Si depending on the number of contacts both in the glove box and under ambient conditions. Large fluctuations are detected for the samples in the glove box, so the measurement number is set as 256. The fluctuation of etched Si in the glove box (40.07±12.10 nN) is larger than that under ambient conditions (107.7+2.6 nN). The adhesion force of etched Si under ambient conditions increases to the maximum and then decreases with the increase of the measurement number. Also, the fluctuation of grooved Si in the glove box (33.15±20.02 nN) is larger than that under ambient conditions (69.1±10.4 nN). However, under both conditions, the adhesion forces of grooved Si increase suddenly and then decrease with the increasing of the measurement number.

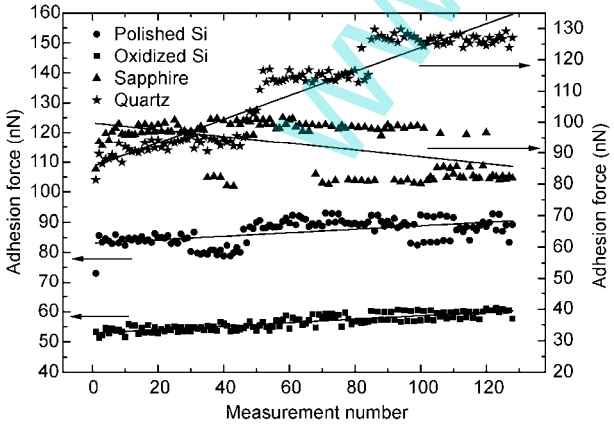

Figure 8 Adhesion force versus sequential measurement number in the glove box.

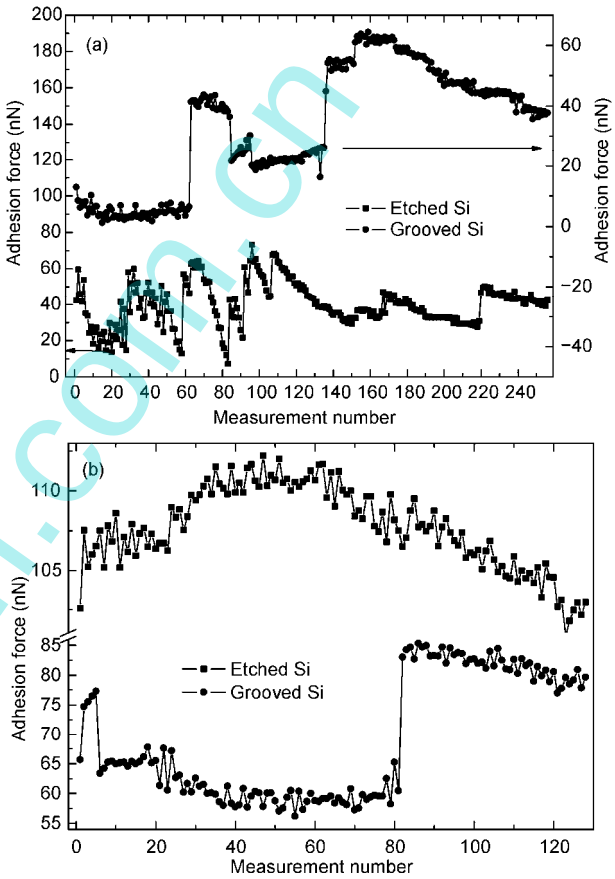

Figure 9 Adhesion force versus sequential measurement number for etched Si and grooved Si in the glove box and under ambient conditions. (a) In the glove box; (b) under ambient conditions

Figure 10 shows the adhesion variations of quartz and oxidized Si depending on the number of contacts under distilled water. With the increase of the measurement number, the adhesion forces of quartz increase slightly, but are with large fluctuations (7.92±2.68 nN). However, the adhesion forces of oxidized Si (9.11±5.11 nN) are divided into two parts (near 2 and 12 nN, respectively), which are with small fluctuations.

In the process of recording many force-displacement curves at a single location, the surface topography of the sample contacting with the tip is likely to be changed for different measurements. First of all, the contact when the tip snaps into contact with the sample is slightly different from

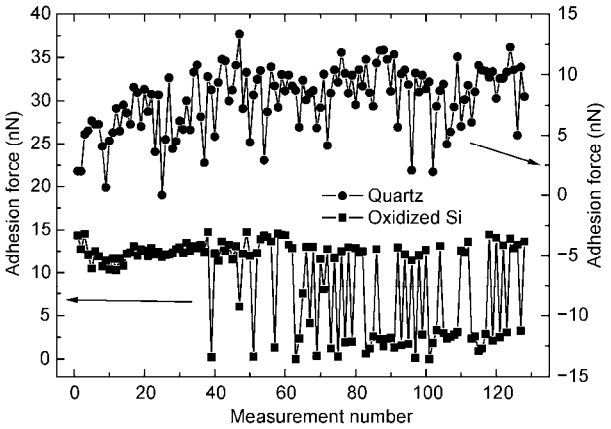

Figure 10 Adhesion force versus sequential measurement number for quartz and oxidized Si under distilled water.

that when the applied load is the maximum. As the cantilever bends upward, the tip will slip slightly in the direction parallel to the cantilever. Secondly, the vertical motion of the scanner cannot be entirely linear (due to creep, hysteresis, aging, etc.). Furthermore, the stability also depends on the mechanical and electronic factors of the AFM (such as vibration, thermal drift, noise, etc.). Therefore, during a series of measurements, the measured area of the sample should be larger than the area of the tip. As shown in Figures 8 and 9, the adhesion forces of the etched Si and grooved Si exhibit larger fluctuations than others. This is because they are rougher than others. The variation of the topography leads to the variation of contact area, and ultimately leads to the fluctuations of the adhesion forces. As for polished Si and oxidized Si, the variations of contact areas are small due to smooth surfaces, resulting in relative stable adhesion forces.

The plastic deformation or damage of the asperities on the surface will lead to the increase of contact area. Then the adhesion forces will steppedly increase with the increasing of the measurement number. The adhesion forces of quartz in Figure 8 and that of grooved Si in Figure 9 are the examples. This plastic deformation or damage is most likely due to fatigue rather than the yield limit of the asperities. Because in the experiments, plastic deformation was still not observed when the load was about 400 nN, as described in Section 3.4.

3.4 Dependence of adhesion forces on external loads

To study the dependence of adhesion force on external load, the applied load between the tip and sample can be varied by changing the maximum voltage of the scanner. The purpose of these tests is to see if the asperities undergo any plastic deformation during the experiments. In all the figures in this section, a series of adhesion force measurements at the same location are shown where the load is first increased (full symbols) and then decreased (open symbols). The experiments were carried out in a glove box, under ambient conditions (after being taken out of the glove box and exposure for two hours) and under distilled water. The contact time was also 0 s.

Figure 11 shows the dependence of adhesion force of polished Si and sapphire on loading force in the glove box. With increasing load, the adhesion forces of them increase slightly. And the adhesion forces decrease with decreasing load. The adhesion forces of polished Si are almost the same with increasing and decreasing load. Meanwhile, the adhesion forces of sapphire with decreasing load are less than those with increasing load.

Figure 12 shows the dependence of adhesion force on applied load for etched Si and grooved Si in the glove box and under ambient conditions. The variations of the adhesion forces are similar to those described above. However, in the glove box, the adhesion force of etched Si increases suddenly when the load is about 230 nN. The large adhesion force does not hold all the time. When the load is about 290 nN, it begins to decrease. With decreasing load, the large adhesion force does not exist.

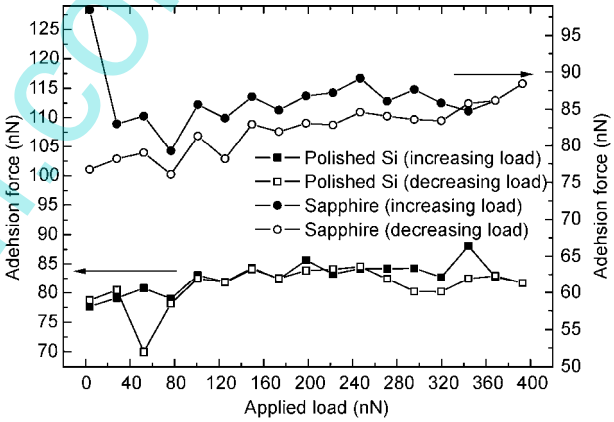

Figure 11 Adhesion force versus applied load for polished Si and sapphire in the glove box.

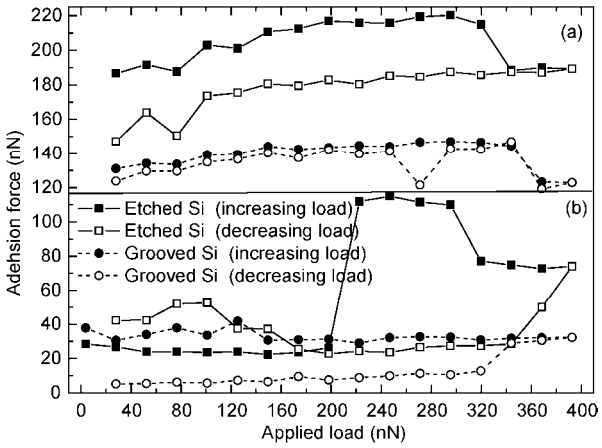

Figure 12 Adhesion force versus applied load for etched Si and grooved Si in the glove box and under ambient conditions. (a) Under ambient conditions; (b) in the glove box.

Figure 13 shows the dependence of adhesion force on applied load for oxidized Si and quartz in the glove box and under distilled water. With increasing load, in the glove box, the adhesion force of quartz increases, while the adhesion force of oxidized Si fluctuates to some extent without any increasing tendency. Also, under distilled water, the adhesion forces of both of them remain relatively stable without any increasing tendency.

The contact area induced by elastic deformation between the tip and the sample is due to the applied load and the adhesion energy. With the increase of the normal load, the deformation increases, leading to increased contact area and adhesion force. The elastic deformation is recovered once the tip is removed from the sample, before the next measurement is made. Therefore, with the decrease of the load, the adhesion forces decrease too, rather than remaining at the maximum adhesion. The adhesion forces will not decrease with the decrease of the load if the plastic deformation of nano-irregularities happens. Hence, a plastic deformation is probably negligible in these experiments. The maximum applied load is only ~400 nN. For one thing, the accessible largest applied load is limited by the normal spring constant of the cantilever (0.135 N/m used). For another, large bending deformation of the cantilever is avoided because of reducing the lateral movement of the tip.

3.5 Dependence of adhesion force on contact time

When the maximum voltage of the scanner is reached, the contact between the tip and sample can be kept for some time. The influence of the contact time on the adhesion force at a single location at a constant load was studied in a range of 1 to 10 s. The experiments were carried out in a glove box, under ambient conditions (after being taken out of the glove box and exposure for two hours) and under distilled water. The applied load was ~220 nN.

Figure 14 shows the dependence of adhesion force on contact time in the glove box. With the increase of contact time, the adhesion force of grooved Si exhibits strong fluctuation which is likely due to the roughness of the surface.

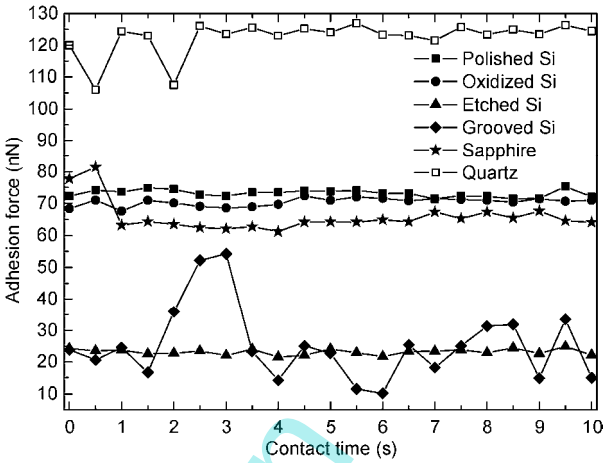

Figure 14 Adhesion force versus contact time for all the samples in the glove box.

The adhesion forces of other samples remain relatively stable without large fluctuations. The mean adhesion forces and standard deviations of samples 1–6 are 73.14 ± 1.12, 70.42 ± 1.27, 23.14 ± 0.92, 25.25 ± 11.69, 65.77 ± 4.90 and 122.45 ± 5.47 nN, respectively.

Figures 15 and 16 show the dependence of adhesion force on contact time under ambient conditions and under distilled water. A general increase in the adhesion force with contact time was observed. The mean adhesion forces and standard deviations of etched Si and grooved Si are 241.03±4.79 and 123.23±1.60 nN under ambient conditions, while those of oxidized Si and quartz are 19.0±1.2 and 8.3±2.7 nN under distilled water.

The variation of adhesion force affected by contact time in the glove box is different from those under ambient conditions and under distilled water. This may result from

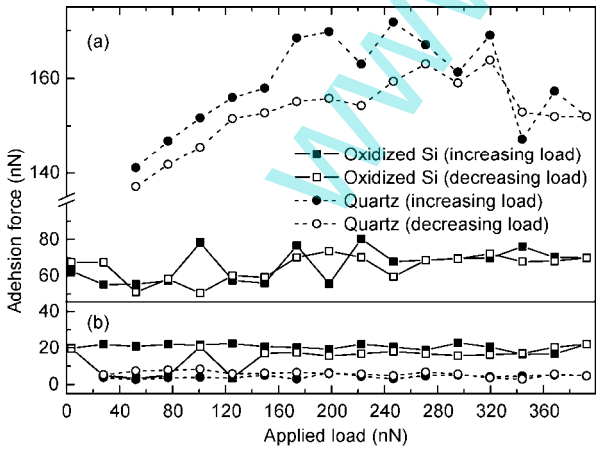

Figure 13 Adhesion forces versus applied loads for quartz and oxidized Si in the glove box and under distilled water. (a) In the glove box; (b) Under the water.

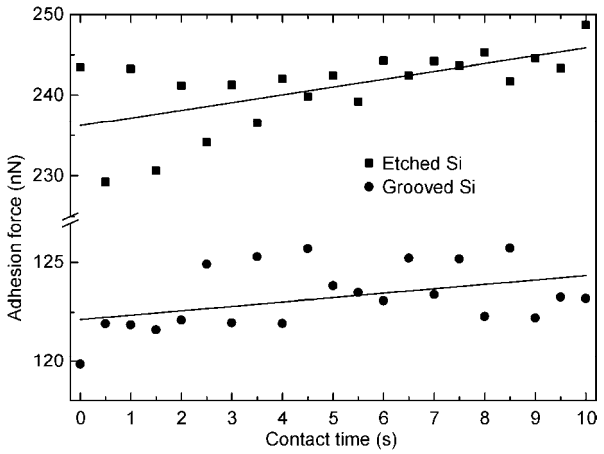

Figure 15 Adhesion force versus contact time for etched Si and grooved Si under ambient conditions.

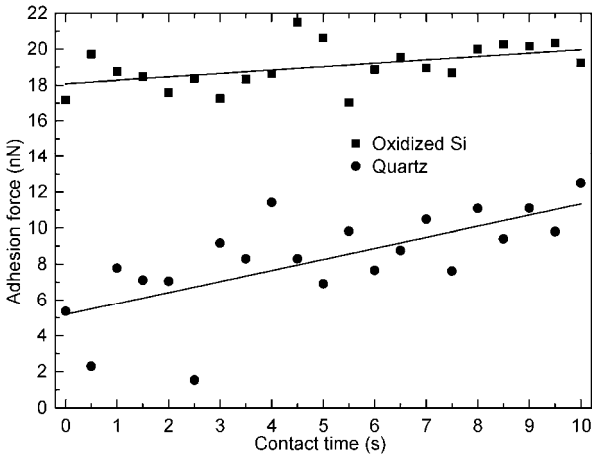

Figure 16 Adhesion force versus contact time for oxidized Si and quartz under distilled water.

different dominant components of the total adhesion force under different conditions. In the glove box, the adhesion force is mainly from the electrostatic and vdW forces. Under distilled water, the adhesion is mainly from the vdW force. Under ambient conditions, the dominant component of adhesion is the capillary force. The vdW force exists, but it is much smaller. Under ambient conditions, the formation of liquid bridges may become easier with longer contact time, resulting in larger adhesion.

3.6 Adhesion forces under different conditions

For the convenience of discussion, the experimental procedure will be outlined here. In order to obtain mean adhesion force and distribution for each sample, 1024 locations were selected in a scanning area 60 μm×60 μm.

The force-displacement curve was recorded in each location, and the adhesion data was extracted automatically by using a short FORTRAN program. The experiments were carried out in the glove box, under ambient conditions, under distilled water, and under KCl solution, sequentially.

The samples were first placed into the glove box. Two hours later, the experiments were performed. The adhesion forces of samples 1–6 were measured in turn. It took about two hours to test a sample. After being taken out of the glove box, the samples were placed in the air for two hours. Then the experiments under ambient conditions were carried out. We got the adhesion data of the etched Si and grooved Si. However, the adhesion forces of the other four were so large that they were beyond the measuring range of the probe. Then, the etched Si and grooved Si were exposed to the air for three days. The two samples were ultrasonically cleaned in an alcohol solution for 15 minutes, and then ultrasonically cleaned in the distilled water for 15 minutes. After drying, we got the adhesion data of the two samples again. After exposure to the air for 10 hours, we obtained the adhesion data of the two samples once again. At last, the experiments were performed under distilled water, and under KCl solution, sequentially. Before showing the distributions of adhesion forces, the mean adhesion forces and standard deviations under different conditions are given first, as shown in Table 4.

3.6.1 Adhesion forces in the glove box

Figure 17 shows adhesion force histograms of the samples measured in the glove box. Each of them exhibits a Gaussian-like distribution (fitting curves displayed in the figure). From the figure, the mean adhesion forces of the samples are very different from one another. However, from Table 3, there are no significant differences among the surface energies of the samples. It seems that the theory of thermodynamic surface free energy cannot predict the adhesion force between two parallel solid surfaces.

The free energy of the solid surface can be calculated by the contact angles between the probe liquids and the surface. Then, the interfacial energy between the tip and the sample can be worked out if the surface free energy of the tip is known. The work of adhesion can be obtained by the relationship of the interfacial energy and the work of adhesion. When the probe tip is in nano-scale, this method is proved to be reasonable. However, this method is not suitable for adhesion between two parallel solid surfaces. This may be caused by different contact geometries. When the tip is small, the tip and sample are in single-asperity contact. However, the tip and sample are in multi-asperity contact, when using a blunt tip.

Table 4 Mean adhesion forces and their standard deviations under different conditions

Sample	Under KCl solution (nN)	Under distilled water (nN)	In the glove box (nN)	Under ambient conditions (nN)
Polished Si	0.59±0.72	5.2±9.3	48.9±26.3	–
Oxidized Si	1.1±2.0	16.5±8.5	91.0±25.7	–
Etched Si	0.58±1.02	9.5±14.5	49.2±25.0	171.7±46.5 [a] *130.4±71.1* [b] **16.0±9.6** [c]
Grooved Si	–	0.35±1.56	29.3±17.2	92.0±40.1 [a] *101.7±50.9* [b] **65.9±40.3** [c]
Sapphire	0.42±0.81	6.8±6.6	116.4±33.2	–
Quartz	0.043±0.069	2.6±2.4	52.3±17.5	–

Note: a) Data from experiments after being taken out of the glove box and exposure for two hours; b) data from experiments after exposure for 3 days and ultrasonically cleaning; c) data from experiments after exposure to the air for 10 hours.

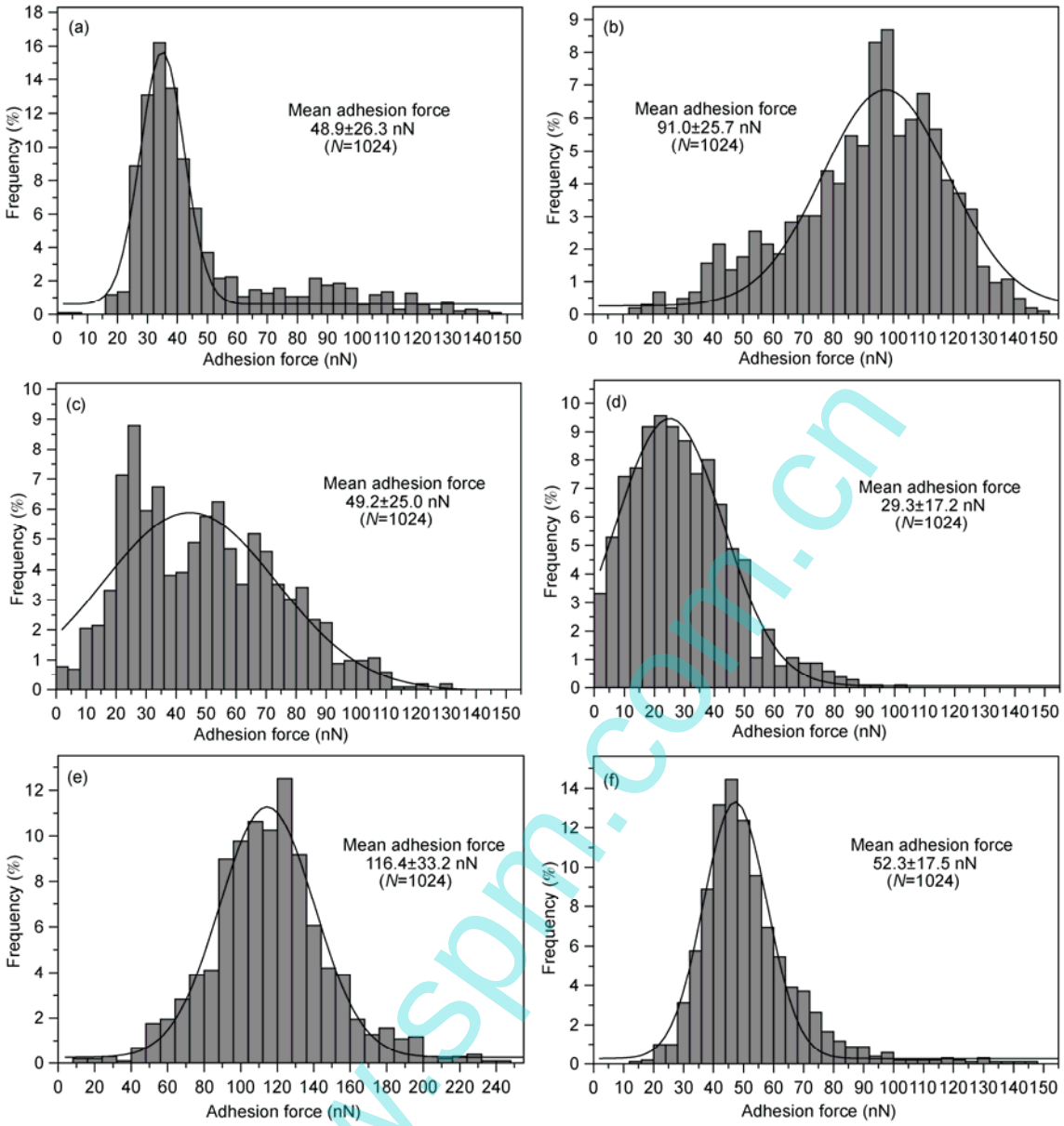

Figure 17 Histograms of the adhesion forces for all the samples in the glove box. (a) Polished Si; (b) Oxidized Si; (c) Etched Si; (d) Grooved Si; (e) Sapphire ; (f) Quartz.

Generally speaking, surface roughness decreases the actual area of contact, leading to the lower adhesion force. From Figure 17, the mean adhesion force of polished Si (R_q = 1.41 nm) is about twice as large as that of grooved Si (R_q = 37.6 nm). In Figures 17 (a) and (b), the adhesion forces less than 12 nN are rarely found. However, in Figures 17 (c) and (d), the adhesion forces less than 12 nN account for 3.5% and 16.0%, respectively. All of these indicate that surface roughness reduces the adhesion force. However, the mean adhesion force of oxidized Si (R_q = 1.1 nm) is about twice as large as that of polished Si, although the roughness of them are close to each other. Similarly, the mean adhesion forces of polished Si and etched Si are almost the same, although the roughness of etched Si is much larger (R_q=21.9 nm). This shows that surface roughness is only a factor affecting the adhesion. There are other factors that also have an impact on the adhesion force.

In the glove box, the filled nitrogen is unmixed and dry. Under the conditions, the electrostatic forces play an important role in the adhesion. The magnitude of electrostatic force is related to the number of charges. The number of charges is related to the length of time storing in the glove box. The longer time, the more charges. When testing, there are more charges on oxidized Si, etched Si and grooved Si than that of polished Si, since they were tested after polished Si. Therefore, they should have larger mean adhesion forces. That is, if no electrostatic force exists, the mean adhesion force of grooved Si should be much smaller. This is

proved by the experiments under distilled water. Generally, there is no electrostatic force when testing under distilled water. It can be seen from Table 4 that the mean adhesion force of polished Si is 5.2 nN, while that of grooved Si is only 0.35 nN.

However, long-range electrostatic forces were not found from force-displacement curves of the first five samples. The influence of electrostatic charges may be short-range when testing these samples. The long-range electrostatic forces were found when testing quartz. The long-range electrostatic forces can be seen from all the 1024 force-displacement curves clearly. Figure 18 shows the force-displacement curves of quartz in different conditions and force-displacement curve of sapphire in the glove box.

The force-displacement curve shown in Figure 18(b) was recorded at the end of experiments in the glove box. Even at that time, the long-range electrostatic forces were not detected on sapphire. It can be clearly seen from Figure 18 (a) that the cantilever bends downward by sensing attractive forces, even when the tip is far away from the sample. After the tip snaps out of contact with the sample, the cantilever goes back to its original starting position slowly, because of the long-range attractive forces. However, long-range electrostatic forces were not found on quartz when testing under ambient conditions and under distilled water, as shown in Figures 18(c) and (d).

The surface of quartz is very smooth (R_q=1.96 nm), and the long-range attractive force exists between the contact of the tip and quartz. However, the adhesive forces recorded are not very large, as shown in Figure 17. It is most likely because the long-range attractive forces do not contribute to the total adhesion force. There are many charges on the surface of quartz. However, the charges on the sample are opposite to the charges on the tip. By contacting, the neutralization of the positive and negative charges occurs.

3.6.2 *Adhesion forces under ambient conditions*

Figure 19 shows the adhesion distributions of etched Si and grooved Si under different treatments and conditions. Each of them exhibits a Gaussian-like distribution (fitting curves displayed in the figures). This may be related to the normal distribution of surface height. Under different treatments and conditions, the adhesion force becomes different, indicating that the adhesion force is influenced by many factors. For example, the mean adhesion force of etched Si shown in Figure 19(a) is about an order of magnitude larger than that shown in Figure 19(e).

Under ambient conditions, the surface would be covered by a thin water film and easy to form capillary meniscus by the adsorbed water molecules. Therefore, the capillary force will always be present. After being taken out of the glove box and exposure to the air for two hours, the samples were contaminated by particles of dust in the air, which would lead to small capillary forces. However, the electrostatic charges might be still on the surfaces of the samples. Although influenced by the contamination, the contributions of adhesion force are the capillary force, electrostatic force and vdW force, which lead to large adhesion force, as shown in

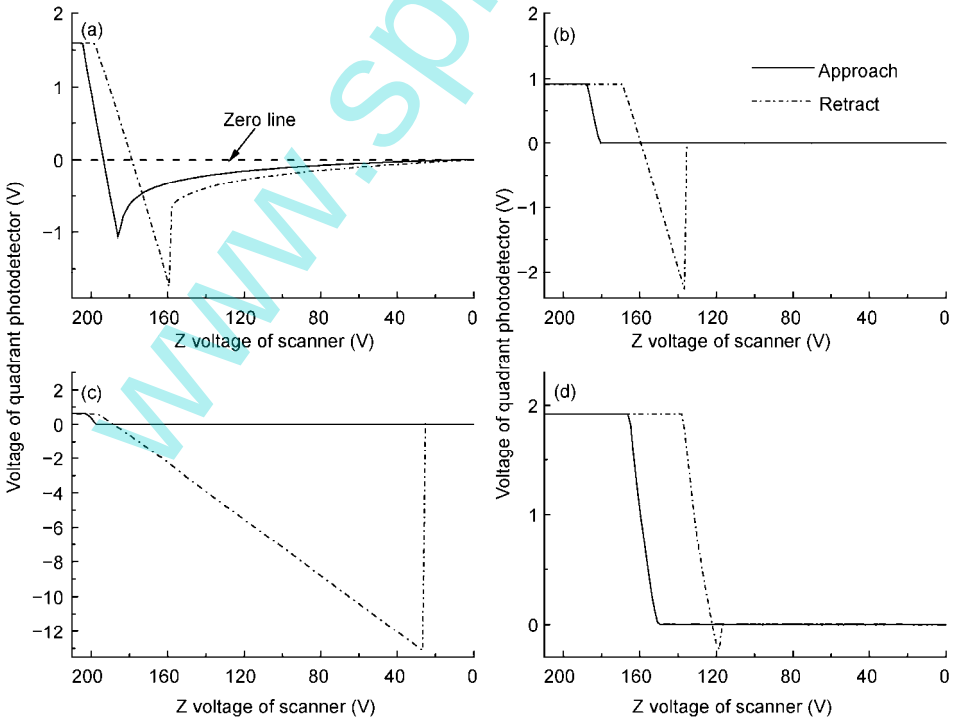

Figure 18 Force-displacement curves of quartz in different conditions and force-displacement curve of sapphire in the glove box. (a) Quartz in the golve box; (b) sapphire in the golve box; (c) quartz under ambient conditions; (d) quartz in the water.

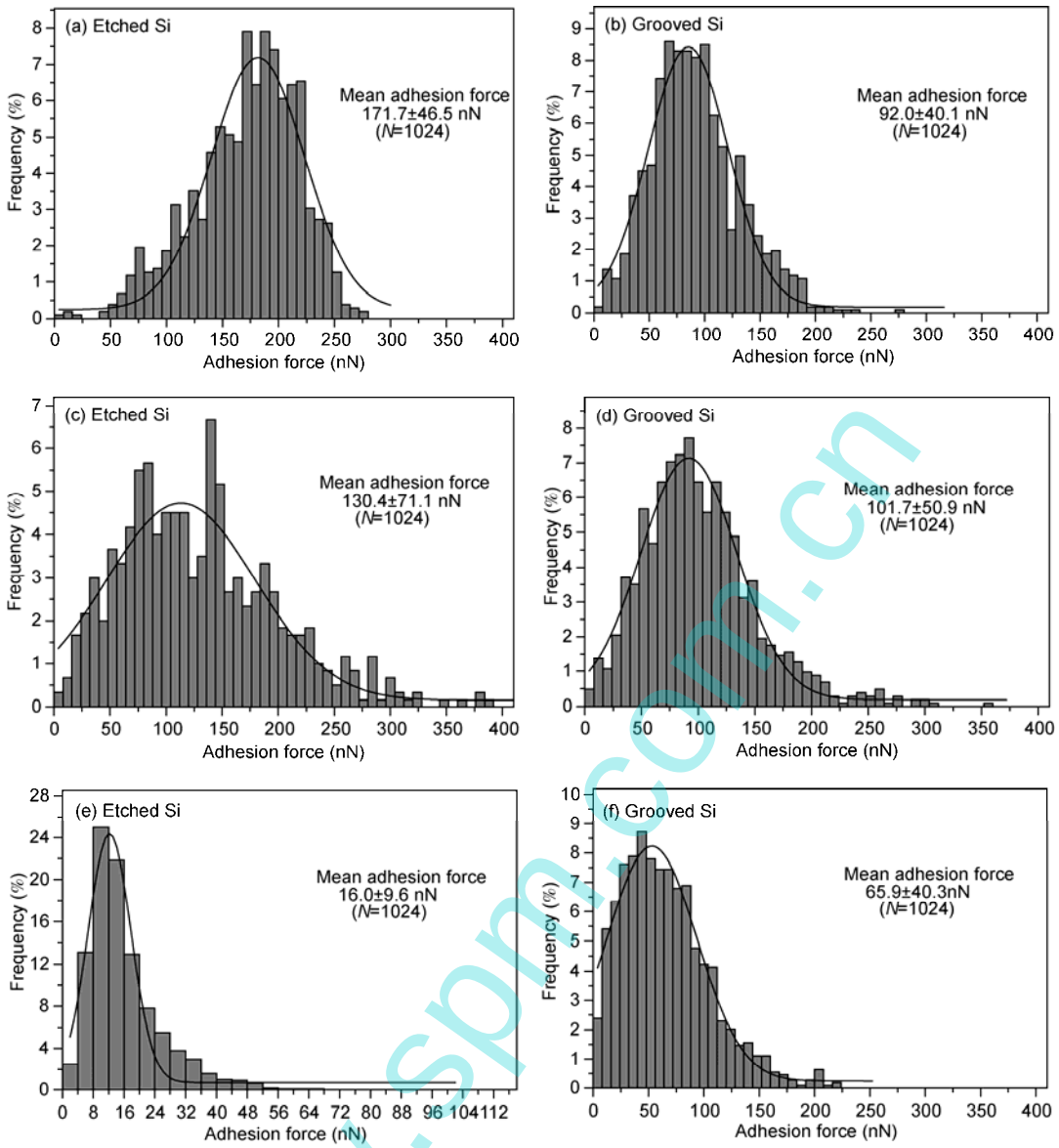

Figure 19 Histograms of the adhesion forces of etched Si and grooved Si after being taken out of the glove box and exposure to the air for two hours (a, b), after exposure to the air for 3 days and ultrasonically cleaning (c, d), and after cleaning and exposure to the air for 10 hours (e, f).

Figures 19(a) and (b). After exposure for 3 days to the air, the electrostatic charges might be eliminated or there were few charges on the surfaces. By ultrasonically cleaning, the factor of contamination could be removed. Without the contamination, the capillary force and vdW force can also lead to large adhesion, as shown in Figures 19(c) and (d). However, with the contamination, the adhesion force can be smaller, as shown in Figures 19 (e) and (f). It was expected that the mean adhesion force shown in Figure 19(f) would be smaller than that shown in Figure 19(e), since the roughness of groove Si is larger. However, we got an opposite result. This may be because there are some electrostatic charges on the surface of groove Si at that time. Base on the discussion above, we can safely come to the conclusion that the contamination by particles of dust is an important factor, and should always be considered when investigating the adhesion force in the air. And, like adhesion in the glove box, the electrostatic force may also become an important contribution to the adhesion force under ambient conditions.

Figure 20 shows a force-displacement curve of etched Si measured after being taken out of the glove box and exposure to the air for two hours. When the Z-direction voltage of the scanner is about 194 V, the voltage of quadrant photodetector decreases suddenly, and then increases again. This may indicate the damage of asperities on the surface. A polyline is shown in the figure, since the number of collected voltages is only 150. The height of asperities (~48 nm) can be calculated by multiplying the corresponding voltage of the polyline by the extension coefficient of the scanner in the Z direction. Admittedly, as shown in Figure 5 (c), there are some small asperities on the surface of etched Si.

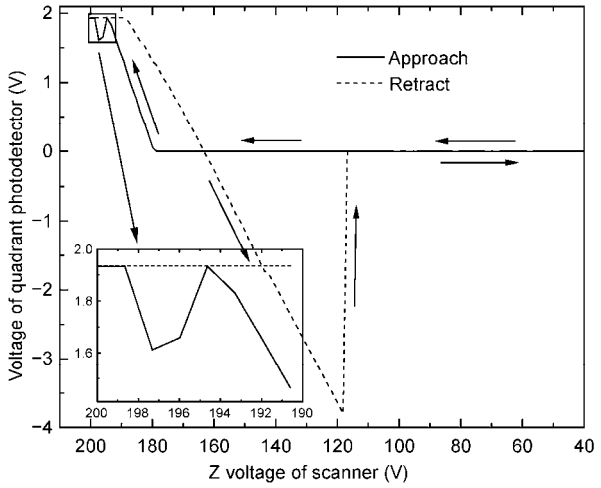

Figure 20 A force-displacement curve of etched Si measured under ambient conditions.

3.6.3 *Adhesion forces under distilled water*

Figure 21 shows the adhesion force distributions of the samples measured under distilled water. Only the adhesion forces of oxidized exhibit a Gaussian-like distribution (fitting curve displayed in the figure). The adhesion forces of polished Si, etched Si, grooved Si and sapphire have a large proportion near zero. Among them, the adhesion forces of sapphire are evenly distributed in the range of 1–11 nN. The adhesion forces of quartz are relatively concentrated. The proportion of adhesion forces in the range of 0–6 nN are 95.1%.

The mean adhesion forces under distilled water can be compared with that in the glove box from Table 4. It can be found that the mean adhesion force of grooved Si under distilled water reduces to about 1/84 of that in the glove box. Meanwhile the mean adhesion forces of sapphire and quartz reduce to 1/17 and 1/20, respectively. Under distilled water,

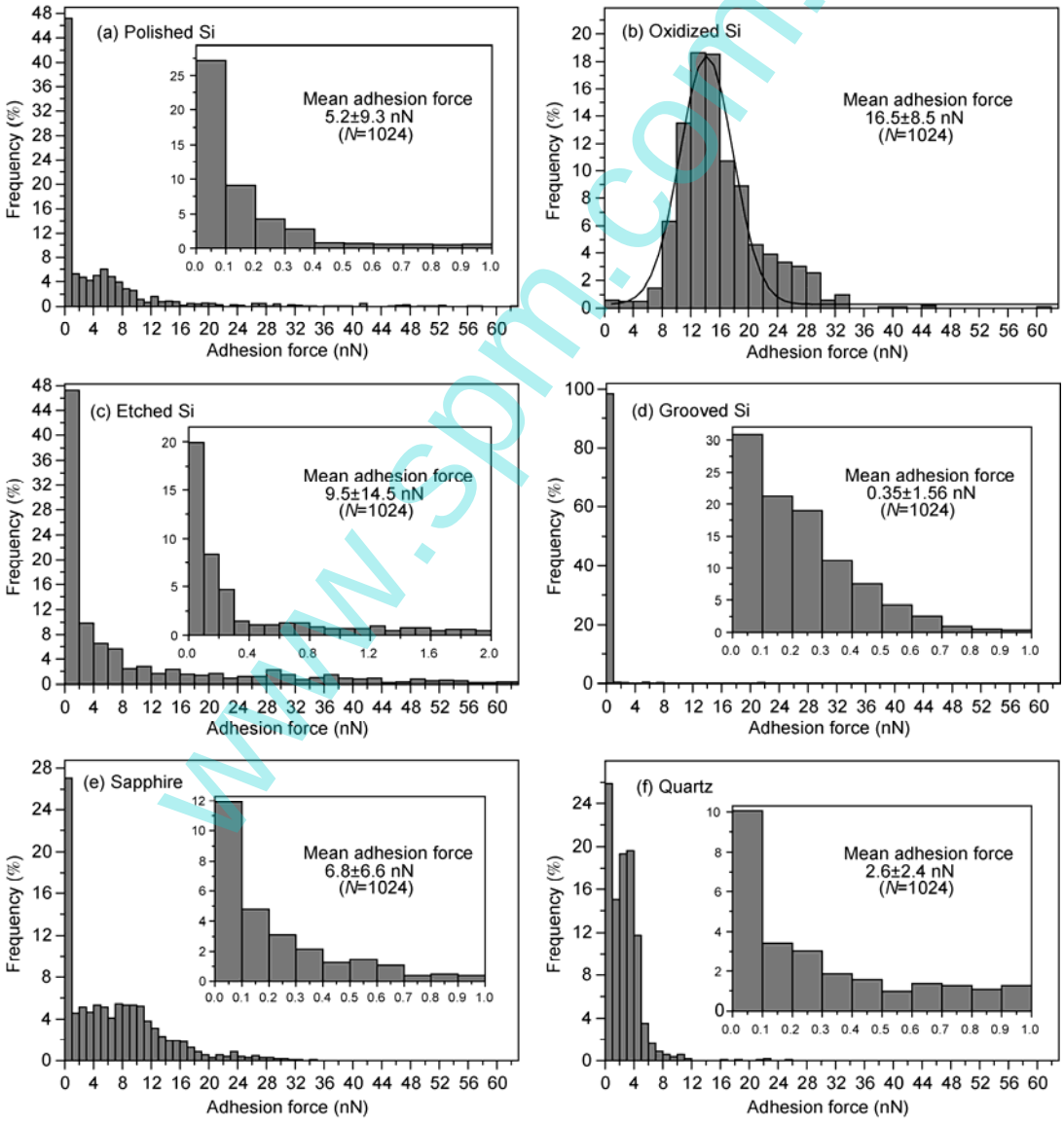

Figure 21 Histograms of the adhesion forces for all the samples under distilled water.

the mean adhesion force of oxidized Si is three times as large as that of polished Si.

Under distilled water, the general rule of roughness effects on adhesion force (large roughness leads to small adhesion) holds. For example, the mean adhesion force of polished Si is 5.2 nN, while that of grooved Si is 0.35 nN. However, by comparing Figures 21(a) and (c), the distribution of adhesion forces of etched Si in the range of 16–50 nN is larger than that of polished Si in the same range. In addition, the mean adhesion force of etched Si is about twice as large as that of polished Si. In other words, the adhesion forces of etched Si are larger with larger roughness. The arguments are internally contradictory.

This phenomenon can be understood by the fact that there are some nano-scale bubbles on the surface. There were some bubbles on the surface of etched Si, leading to a larger mean adhesion force. However, there was no bubble on the surface of grooved Si. The presence of these bubbles was detected by some adhesion force measurements [34-37]. The nanobubbles were confirmed by the phase shift image obtained in noncontact tapping mode of AFM [38].

In the experiments, the existence of bubbles was also detected. Figure 22 shows four sequential force-displacement curves of quartz measured on the four consecutive locations under distilled water. The distance between the locations is approximately 500 nm. The strange phenomenon shown in Figures 22 (b)–(d) is not found in the force-displacement curves after Figure 22 (d). In addition, other force-displacement curves are all similar to Figure 22 (a), where the snapping into contact is obviously not recorded, and the voltage of quadrant photodetector increases directly from zero up to the maximum. Meanwhile, in Figures 22 (b)–(d), with the increasing of normal load, the voltage of quadrant photodetector increases first, and then decreases suddenly, then increases again. It is obvious that the tip is pressed by an object first. Then the object cannot afford to the increased normal load, resulting in the crush of the object. After that, the tip and sample come into contact with each other, and the voltage of quadrant photodetector increases again. Since this phenomenon is from four sequential force-displacement curves, and the objects are growing from small to large, this object should not be asperities or other contaminants. It is most likely that the objects are bubbles. The small bubble is adsorbed at the bottom of the tip. The small bubble is pressed to the edge of the tip, when the tip and sample are in contact. After the tip jumps off the sample, the bubble goes back to the bottom of the tip. With the tip being dragged onto next location, the bubble is growing. In Figure 22 (d), the maximum height of bubble (~254 nm) can be calculated by multiplying the corresponding voltage of convex portion on the horizontal axis by the extension coefficient of the scanner in the Z direction. The bubbles found here are similar in size to those observed in the literature (150–400 nm of radius and 60–200 nm of height) [38].

3.6.4 Adhesion forces under KCl solution

The adhesion forces were also measured under KCl solution. The zero lines of the force-displacement curves obtained under KCl solution exhibit strong fluctuations. This can lead to the inaccurate measurement of the adhesion force to some extent. When measuring grooved Si, the adhesion forces were very small. To avoid wrong calculation of adhesion by the FORTRAN program, we did not continue the measurements. Therefore, the adhesion distribution of grooved Si is not available. And we can regard the mean adhesion force of grooved Si as zero. The adhesion force

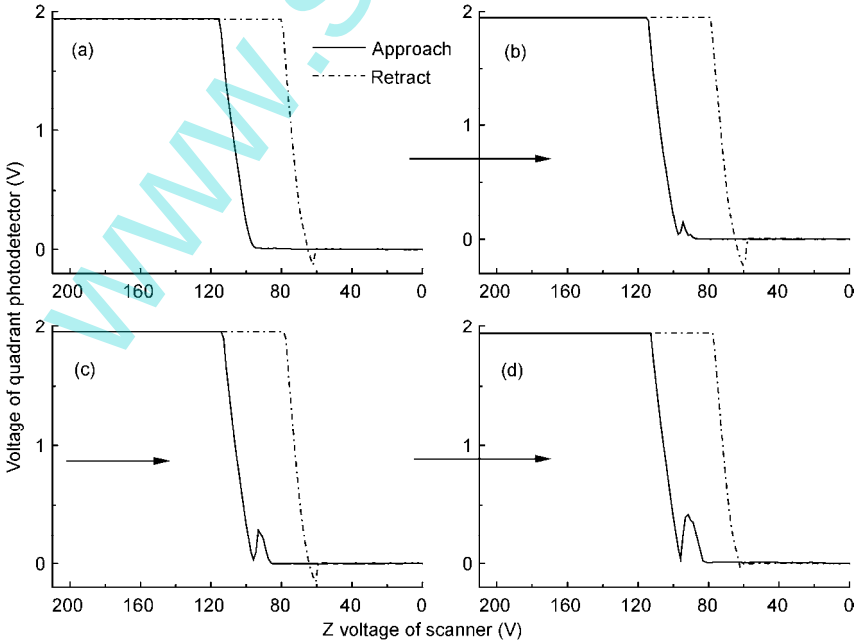

Figure 22 Four sequential force-displacement curves of quartz measured under distilled water.

distributions of the other five samples measured under KCl solution are shown in Figure 23.

As shown in the figure, the adhesion forces of the samples all have a large proportion near zero. The mean adhesion forces under KCl solution can be compared with those under distilled water from Table 4. It can be found that the mean adhesion force of quartz under KCl solution reduces to about 1/60 of that under distilled water. The mean adhesion force of etched Si and sapphire reduces to about 1/16 of that under distilled water, while the mean adhesion forces of polished Si and oxidized Si reduce to 1/9 and 1/15, respectively. By introducing the KCl, the adhesion force can be changed by an order of magnitude. This may be due to a repulsive force existing between the tip and sample.

When two charged surfaces are separated by a thin layer of an electrolyte solution, the contributions of adhesion are primarily the vdW force and electrostatic double-layer force [39]. The electrostatic double-layer force arises because of surface charges at interfaces. Surface charges are induced on both surfaces of the tip and sample, because of the dissociation or adsorption of charged species. The surface charges are balanced by dissolved counterions, which are held together close to the surfaces, forming two electric double-layers. When the surfaces come into contact, the double-layers are perturbed, and the resulting force is known as the electrostatic double-layer force [6]. When the charges of the approaching surfaces have the same sign, the concentration of ions between the surfaces always increases. This results in a repulsive force [40].

3.7 Estimation of real contact area

The vdW force can be calculated by the geometrical features of the bodies and the Hamaker constant which includes all physico-chemical information. The vdW force between two flat surfaces can be calculated by [41]

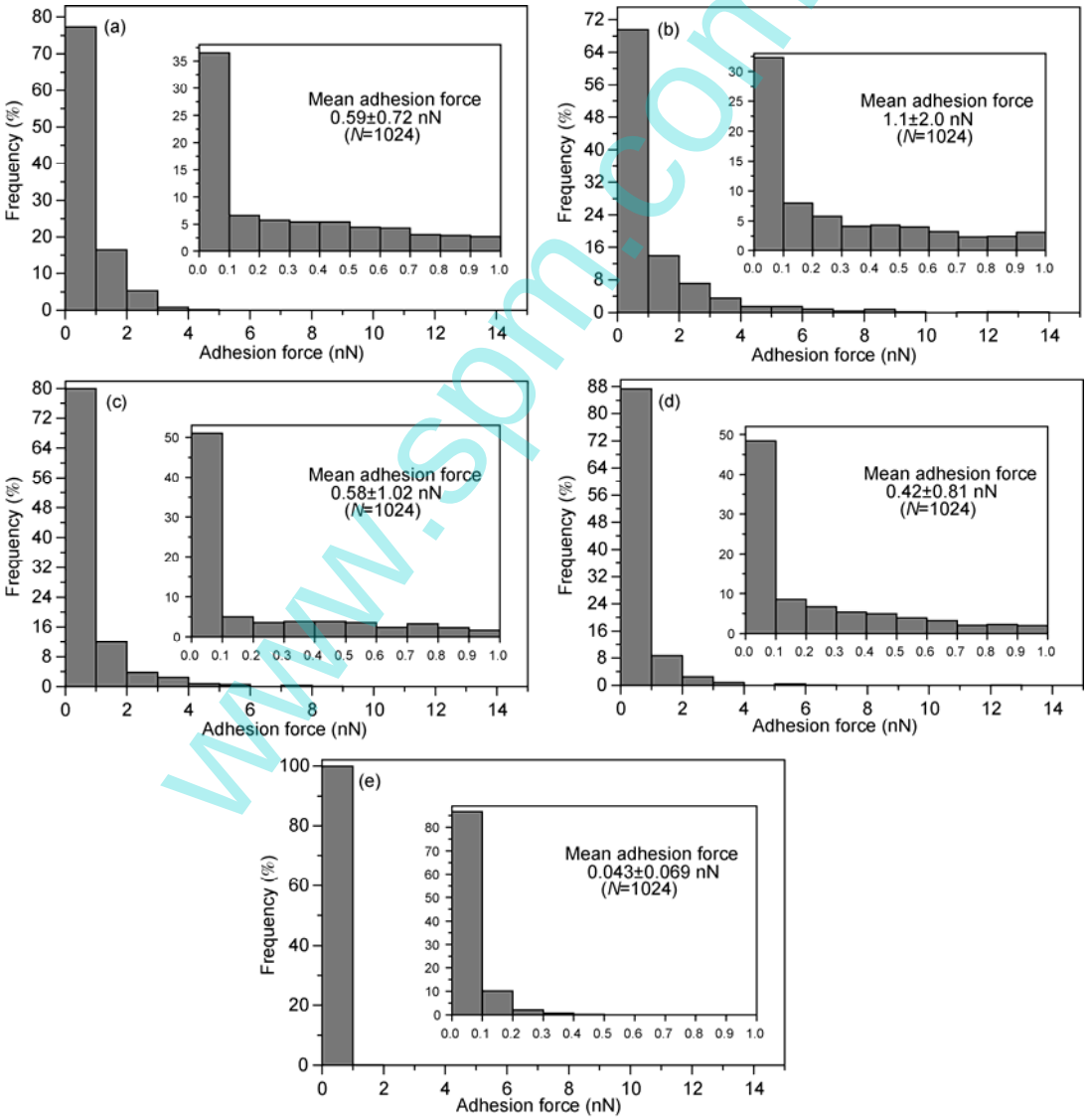

Figure 23 Histograms of the adhesion forces for the samples under KCl solution. (a) Polished Si; (b) Oxidized Si; (c) Etched Si; (d) Sapphire; (e) Quartz.

Table 5 The calculation of real contact area and the ratios of the real contact area to apparent contact area. The Hamaker constants were calculated by Senden and Drummond [42]

System	A_H ($\times10^{-20}$ J)	$\langle F_{ad}\rangle$ (nN)	S_{real} (nm^2)	S_{app} (nm^2)	S_{real}/S_{app}
Silicon/air/silicon	18.65	48.9	22.2	2.35×10^6	~1/(1.0×10^5)
Silicon/water/silicon	9.75	5.2	4.52	2.35×10^6	~1/(5.2×10^5)
Silicon/air/silica	10.26	91.0	75.1	2.35×10^6	~1/(3.1×10^4)
Silicon/water/silica	1.92	16.5	72.8	2.35×10^6	~1/(3.2×10^4)

$$F_{vdW}=\frac{A_H}{6\pi {D_0}^3}S_{real}, \tag{11}$$

where A_H is the Hamaker constant between two contacting bodies, D_0 is the cut-off distance and S_{real} is the real contact area. The mean value of D_0 as 0.165 nm recommended by Israelachvilli is used here [41]. It is assumed that the adhesion forces of polished Si and oxidized Si measured in the glove box and under distilled water are totally the vdW forces, and eq. (11) can be used in these systems. As shown in Table 5, the mean adhesion forces $\langle F_{ad}\rangle$ of polished Si and oxidized Si are used to estimate the real contact area. The real contact area can be calculated by eq. (11). The apparent contact area between the flat tip and the surface is $S_{app}=\pi d^2/4=2.35\times10^6\,\mathrm{nm}^2$, where d is the diameter of the tip. The ratios of the real contact area to apparent contact area are listed in the table. It shows that the real contact area when the tip jumps off the sample is only a small proportion of the apparent contact area.

4 Conclusions

By the contact angle experiments, there are no significant differences among the surface energies of the samples. However, under different conditions, the mean adhesion forces of the samples are all very different from one another. This is very likely caused by the multi-asperity contact between two micro-scale parallel solid surfaces. For this contact, the real contact area without the applied load is only a small proportion of the apparent contact area. And the adhesion force cannot be predicted by the theory of thermodynamic surface free energy.

The measurement stability and repeatability of adhesion by the AFM depend on the surface characterization, measurement methods and the environment. Numerous measurements on the same location will not affect the adhesion greatly if the surface is smooth enough, but may lead to increased adhesion due to the plastic deformation or damage of the asperities. The increasing applied load will increase the adhesion because of larger elastic deformation of the asperities. The increasing contact time will increase the adhesion under ambient conditions and under distilled water, but has little influence on the adhesion in the glove box.

Under different environments, there are different interactions and factors affecting the adhesion force, and the dominant interactions and factors may be different too. The various interactions and factors are mutually coupled to determine the final adhesion force. If the adhesion is mainly from the van der Waals force and/or capillary force, larger roughness will lead to smaller adhesion. In the drying gas and in the air, the electrostatic force could become the dominant interaction. In the air, the contamination by particles of dust is an important factor. Adhesion forces measured under distilled water may be strongly affected by the presence of nanobubbles. Under an electrolyte solution, the electrostatic double-layer force can become a repulsive force, leading to low adhesion.

This work was supported by the National Natural Science Foundation of China (Grant No. 51175182).

1 Zaghloul U, Papaioannou G, Bhushan B, et al. On the reliability of electrostatic NEMS/MEMS devices: Review of present knowledge on the dielectric charging and stiction failure mechanisms and novel characterization methodologies. Microelectron Reliab, 2011, 51: 1810–1818
2 Salimi A. Characterization of nano scale adhesion at solid surface of oxidized PP wax/PP blends. Int J Adhes Adhes, 2012, 33: 61–66
3 Johnson K L, Kendall K, Roberts A D. Surace energy and the contact of elastic solids. Proc R Soc Lond A, 1971, 324: 301–313
4 Derjaguin B V, Muller V M, Toporov Y P. Effect of contact deformations on the adhesion of particles. J Colloid Interface Sci, 1975, 53: 314–325
5 Maugis D. Adhesion of spheres: The JKR-DMT transition using a Dugdale model. J Colloid Interface Sci, 1992, 150: 243–269
6 Butt H J, Cappella B, Kappl M. Force measurements with the atomic force microscope: Technique, interpretation and applications. Surf Sci Rep, 2005, 59(1-6): 1–152
7 Eichenlaub S K. Van der Waals and electrostatic forces in adhesion between irregular particles and surfaces. Dissertation for the Doctoral Degree. Phoenix: Arizona State University, 2003
8 Liu D L, Martin J, Burnham N A. Optimal roughness for minimal adhesion. Appl Phys Lett, 2007, 91(4): 043107
9 vanZwol P J, Palasantzas G, De Hosson J T M. Influence of roughness on capillary forces between hydrophilic surfaces. Phys Rev E, 2008, 78(3): 031606
10 Yaqoob M A, de Rooij M B, Schipper D J. On the transition from bulk to ordered form of water: A theoretical model to calculate adhesion force due to capillary and van der Waals interaction. Tribol Lett, 2013, 49(3): 491–499
11 Martin Y, Abraham D W, Wickramasinghe H K. High-resolution capacitance measurement and potentiometry by force microscopy. Appl Phys Lett, 1988, 52(13): 1103–1105
12 Erlandsson R, Hadziioannou G, Mate C M, et al. Atomic scale friction between the muscovite mica cleavage plane and a tungsten tip. J Chem Phys, 1988, 89(8): 5190–5193

13 Guo Y B, Wang D G, Zhang S W. Adhesion and friction of nanoparticles/polyelectrolyte multilayer films by AFM and micro-tribometer. Tribol Int, 2011, 44(7-8): 906–915
14 Zhang S, Zhang M, Li K. Adhesion force between aramid fibre and aramid fibrid by AFM. Polym Bull, 2011, 66(3): 351–362
15 Pelin I M, Piednoir A, Machon D, et al. Adhesion forces between AFM tips and superficial dentin surfaces. J Colloid Interf Sci, 2012, 376: 262–268
16 Raj G, Balnois E, Helias M A, et al. Measuring adhesion forces between model polysaccharide films and PLA bead to mimic molecular interactions in flax/PLA biocomposite. J Mater Sci, 2012, 47(5): 2175–2181
17 Fahs A, Louarn G. Plant protein interactions studied using AFM force spectroscopy: Nanomechanical and adhesion properties. Phys Chem Chem Phys, 2013, 15(27): 11339–11348
18 Chen L, Kim S, Wang X D, et al. Running-in process of Si-SiO_x/SiO_2 pair at nanoscale — Sharp drops in friction and wear rate during initial cycles. Friction, 2013, 1: 81–91
19 Grierson D S, Liu J, Carpick R W, et al. Adhesion of nanoscale asperities with power-law profiles. J Mech Phys Solids, 2013, 61(2): 597–610
20 Fischer H R, Gelinck E R M. Determination of adhesion forces between smooth and structured solids. Appl Surf Sci, 2012, 258(22): 9011–9017
21 Kappl M, Butt H J. The colloidal probe technique and its application to adhesion force measurements. Part Part Syst Char, 2002, 19(3): 129–143
22 Ando Y. The effect of relative humidity on friction and pull-off forces measured on submicron-size asperity arrays. Wear, 2000, 238(1): 12–19
23 Ando Y. Effect of contact geometry on the pull-off force evaluated under high-vacuum and humid atmospheric conditions. Langmuir, 2008, 24(4): 1418–1424
24 Ferreira O D S, Gelinck E, de Graaf D, et al. Adhesion experiments using an AFM -parameters of influence. Appl Surf Sci, 2010, 257(1): 48–55
25 Colak A, Wormeester H, Zandvliet H J W, et al. Surface adhesion and its dependence on surface roughness and humidity measured with a flat tip. Appl Surf Sci, 2012, 258(18): 6938–6942
26 Xie J, Xie H F, Liu X R, et al. Dry micro-grooving on Si wafer using a coarse diamond grinding. Int J Mach Tool Manu, 2012, 61: 1–8
27 Gnecco E, Bennewitz R, Pfeiffer O, et al. Friction and Wear on the Atomic Scale. In: Bhushan B, ed. Springer Handbook of Nanotechnology. Heidelberg: Springer, 2010. 923–954
28 Carpick R W, Batteas J, de Boer M P. Scanning Probe Studies of Nanoscale Adhesion between Solids in the Presence of Liquids and Monolayer Films. In: Bhushan B, ed. Springer Handbook of Nanotechnology. Heidelberg: Springer, 2007. 951–980
29 Wen S Z, Huang P. Principles of Tribology. Singapore & Beijing: Wiley & Tsinghua University Press, 2012. 219–222
30 Owens D K, Wendt R C. Estimation of the surface free energy of polymers. J Appl Polym Sci, 1969, 13(8): 1741–1747
31 Fowkes F M. Attractive forces at interfaces. J Ind Eng Chem, 1964, 56: 40–52
32 Shimizu R N, Demarquette N R. Evaluation of surface energy of solid polymers using different models. J Appl Polym Sci, 2000, 76(12): 1831–1845
33 Barber A H, Cohen S R, Wagner H D. Static and dynamic wetting measurements of single carbon nanotubes. Phys Rev Lett, 2004, 92(18): 186103
34 Ishida N, Inoue T, Miyahara M, et al. Nano bubbles on a hydrophobic surface in water observed by tapping-mode atomic force microscopy. Langmuir, 2000, 16(16): 6377–6380
35 Tyrrell J W G, Attard P. Images of nanobubbles on hydrophobic surfaces and their interactions. Phys Rev Lett, 2001, 87(17): 176104
36 Yang J W, Duan J M, Fornasiero D, et al. Very small bubble formation at the solid-water interface. J Phys Chem B, 2003, 107(25): 6139–6147
37 Simonsen A C, Hansen P L, Klosgen B. Nanobubbles give evidence of incomplete wetting at a hydrophobic interface. J Colloid Interf Sci, 2004, 273(1): 291–299
38 Serro A P, Colaco R, Saramago B. Adhesion forces in liquid media: Effect of surface topography and wettability. J Colloid Interf Sci, 2008, 325(2): 573–579
39 Misra R P, Das S, Mitra S K. Electric double layer force between charged surfaces: Effect of solvent polarization. J Chem Phy, 2013, 138(11): 114703
40 Chan D Y C, Mitchell D J. The free energy of an electrical double layer. J Colloid Interf Sci, 1983, 95(1): 193–197
41 Israelachvilli J. Intermolecular and Surface Forces. Singapore: Elsevier Pte Ltd, 2011. 253–255
42 Senden T J, Drummond C J. Surface chemistry and tip-sample interactions in atomic force microscopy. Colloids Surf, A, 1995, 94(1): 29–51